Highest Energy Air Showers and Nuclear Interactions

Akinori Ohsawa

Institute for Cosmic Ray Research, University of Tokyo, Kashiwa, 277-8582 Japan.

(Received October 22, 2001)

We formulate the energy distribution of produced particles in multiple particle production, based on the data of direct observation by accelerator and cosmic-ray experiments. The formulated distribution shows strong violation of the Feynman scaling law both in the forward and central regions, which leads to small inelasticity ($< K > < 0.5$) at high energies. We show that the extrapolation of the formulated distribution does not describe highest energy ($\sim 10^{20}$ eV) air showers. We discuss how large the ambiguity of estimated energy is for the highest energy air showers.

§1. Introduction

According to the data of extremely high energy air showers (EHEAS),[1–3] the energy spectrum of primary cosmic rays appears to extend beyond Greisen-Kuzumin-Zatsepin cut-off energy of $\sim 5\times10^{19}$ eV.[4,5] And various speculations are proposed for it, such as the breaking down of Lorentz transformation, "exotic new kinds of sources, perhaps even involving new particle-physics phenomena or topological space-time defects left over from the Big Bang."[6] The issue is one of the central problems in astrophysics at present, and several huge detectors are under construction or under discussion to observe EHEAS.

The energy of these air showers is estimated by comparing the experimental data with the output of the simulations. In these simulations high energy nuclear interaction — multiple particle production (MPP) — is one of the dominant factors for the nuclear cascade process. Needless to say, the characteristics of nuclear interactions are not established yet at these energies, but are assumed by extrapolating those at low energies.

Therefore it is not meaningless to summarize the nuclear interaction characteristics, based on the data of direct observation, and to examine how the nuclear interaction models, assumed in the simulations, reproduce these experimental data. The examination enables us to discuss how large the ambiguity of the energy estimation of EHEAS is due to our limited knowledge on nuclear interaction characteristics at extremely high energies.

Present paper is formed in the following way. In Section 2 we formulate *empirically* the energy distribution of produced particles in MPP, based on the data of direct observation, because we have no *a priori* guiding principles for the energy distribution except energy conservation. Then we discuss the nuclear interaction characteristics at EHEAS region, extrapolating the formulated distribution. The formulated energy distribution is compared with those of nuclear interaction models, assumed in the simulations which are used widely to follow the cosmic-ray diffusion in the atmosphere. In Section 3 we calculate the size of EHEAS based on the formulated energy distribution of produced particles, in order to examine whether the formulated energy distribution is compatible with EHEAS. The calculation is made analytically because we want not only to *describe* but also to *understand* the development of EHEAS. That is, we want to see in which way the respective characteristics of nuclear interactions affect the development of air showers. Section 4 is devoted to summary and discussion.

§2. Experimental data of direct observation

2.1 Energy distribution of produced particles

According to Feynman the energy distribution of produced particles in MMP is independent of the incident energy $\sqrt{s}$ at high energies,[7] when it is expressed by the variable $x^* \equiv 2p^*_{||}/\sqrt{s}$ ($p^*_{||}$: the longitudinal component of the momentum vector $\boldsymbol{p}^*$ of the produced particle)The quantities with and without an asterisk (*) are those in the center of mass system and in the laboratory system, respectively.. One of the empirical formulae to express the energy distribution of *charged* produced particles is[8]

$$\frac{dN}{dx^*} \equiv \frac{1}{\sigma_{inel}}\frac{d\sigma}{dx^*} = D\frac{(1-x^*)^d}{x^*} \qquad (2.1)$$

$$(D = (d+1)/3 = 1.67,\ d = 4.0)$$

which is called 'the scaling function'.

The Feynman scaling law appeared to be valid up to the energy of $\sqrt{s} = 63$ GeV, the maximum available energy at that time.[9] At still higher energies, however, it is shown by accelerator experiments ($\sqrt{s} =$ 200, 546, 630, 900 and 1800 GeV)[10–13] and by cosmic-ray experiments ($< \sqrt{s} >= 500$ GeV)[14] that the law is violated in the central region and in the forward region, respectively.

To discuss the violation of the law quantitatively, we assume the energy distribution of *charged* produced particles of the following type.[15]

$$\frac{dN^2}{dx^* dp_T} = aD\frac{(1-a'x^*)^d}{\sqrt{x^{*2} + \left(\frac{2\mu}{\sqrt{s}}\right)^2}}\, g(p_T) \qquad (2.2)$$

$$\left(x^* = \frac{2p^*_{\parallel}}{\sqrt{s}},\ \mu \equiv \sqrt{p_T^2 + m_\pi^2} \right)$$

where the parameters a and a' are adjusted to fit the experimental data. The formula reproduces the scaling function of eq.(1) using $a = a' = 1$ and $\sqrt{s} \to \infty$. The parameters a (≥ 1) and a' (≥ 1) express enhancement of the scaling function in the central region and suppression in the forward region, respectively.

The p_T-distribution is

$$g(p_T)dp_T = p_T \ \exp\left(-\frac{p_T}{p_0}\right)\frac{dp_T}{p_0^2} \tag{2.3}$$

with

$$p_0 = \begin{cases} c & (x^* < x_0^*) \\ c\left(\frac{x_0^*}{x^*}\right)^{c'} & (x^* > x_0^*) \end{cases} \tag{2.4}$$

$$(c = 0.2 \text{ GeV}/c,\ c' = 0.57,\ x_0^* = 0.08)$$

According to the p_T-distribution of eq.(3), the average value of p_T, $< p_T >= 2p_0$, becomes smaller in the forward region $x^* > x_0^*$, which is observed by the experiments.[11, 16)]

The distribution of eq.(2) can be transformed easily into the rapidity and pseudo-rapidity distributions, dN/dy^* and $dN/d\eta^*$, which are to be compared with the available experimental data at various incident energies. Hence we can obtain the best-fit values of the scaling violation parameters, a and a', at various incident energies.The data are those of all inelastic events but not only NSD (non-single-diffractive) events. That is,

$\sigma_{inel} = \sigma_{NSD} + \sigma_{SD} = \sigma_{ND} + \sigma_{DD} + \sigma_{SD}$.

where ND, DD and SD stand for "non-diffractive", "double diffractive" and "single diffractive", respectively. According to the data by UA5 Collaboration,[10)] the pseudo-rapidity density of the former is smaller by 10 % than that of the latter in in pseudo-rapidity range of $0 \leq \eta^* \leq 3.5$, and almost equal in $\eta^* \geq 3.5$ at $\sqrt{s} = 546$ GeV. The incident energy dependences of the parameters are expressed as

$$a = \left(\frac{E_0}{A}\right)^{\alpha} \qquad (\alpha = 0.105)$$

$$a' = \left(\frac{E_0}{A}\right)^{\alpha'} \qquad (\alpha' = 0.210) \tag{2.5}$$

where $A = 2.0 \times 10^2$ GeV.

We assume three models, tabulated in Table 1, for the energy distribution of produced particles. Model-2 is the best-fit to the experimental data, while Model-0 and Model-1 are for reference.

Fig. 1 shows how the experimental data are described by the formula of eq.(2) with the parameters of eqs.(5). One can see in the figure that the reproduction is satisfactory by Model-2 and that Model-0 (the Feynman scaling law) cannot reproduce the data both in the central and forward regions. Note that the distribution of Model-0 is slightly energy-dependent, as can be seen in eq.(2).

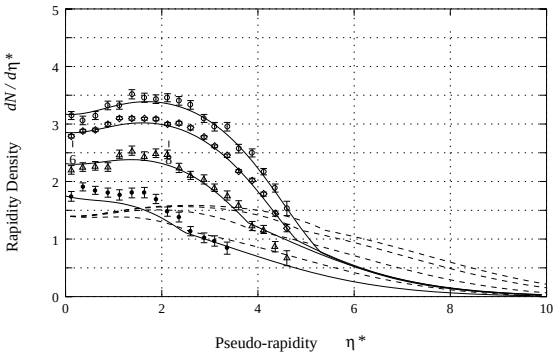

Fig. 1. Pseudo-rapidity density distributions by UA5 Collaboration experiment (plots), those of Model-2 (solid lines) and those of Model-0 (chain lines) at $s^{1/2} = 53$, 200, 546, and 900 GeV. The data are those of all inelastic events (but not only of non-single-diffractive events) at the energies of $s^{1/2} = 53$ GeV (•), 200 GeV (△), 546 GeV (◇), and 900 GeV (○). The solid lines are by Model-2 with the parameter values a' of the best-fitting at respective energies.

2.2 Model-2 at high energies

Since the relation

$$x^* \simeq \frac{E}{E_0} \equiv x$$

is valid approximately at high energies, we can transform the energy distribution of the produced particles, eq.(2), into the one in the laboratory system.

Fig. 2 shows the energy distribution of *charged* produced particles in the laboratory system for various primary energies E_0. The figure shows that the Feynman scaling law is violated strongly both in the central region and in the forward region at high energies. There is almost no particles with $x \geq 0.01$ at $E_0 = 10^{20}$ eV.

Fig. 3 shows the energy dependence of charged multiplicity, given by

$$m(E_0) = \int_0^{1/a'} dx \int_0^{\infty} dp_T \ \frac{aD(1-a'x)^d}{\sqrt{x^2 + \left(\frac{2\mu}{\sqrt{s}}\right)^2}}\ g(p_T)\ ,$$

for the formulated models. One can see in the figure that difference in the multiplicity is small between Model-1 and Model-2 because we have

$$m(E_0) \simeq a\left[\ln\frac{\sqrt{s}}{\mu} - \ln a'\right].$$

That is, the parameter a' appears in the form of $\ln a'$. It is no surprise that the energy dependence of Model-2 agrees better with the experimental data than that of Model-1.

Fig. 3 shows also the energy dependence of the average total inelasticity in the laboratory system, defined by

$$< K > \equiv \frac{3}{2}\int_0^{1/a'} x\,dx \int_0^{\infty} dp_T \ aD\frac{(1-a'x)^d}{\sqrt{x^2 + \left(\frac{2\mu}{\sqrt{s}}\right)^2}}\ g(p_T)$$

Table I. Assumed models

	Scaling violation parameters			
	α	α'	$< K >$	Remarks
Model-0	0	0	const (0.5)	Feynman scaling law
Model-1	0.105	0.105	const (0.5)	
Model-2	0.105	0.210	decreasing	the best-fit to the exp. data

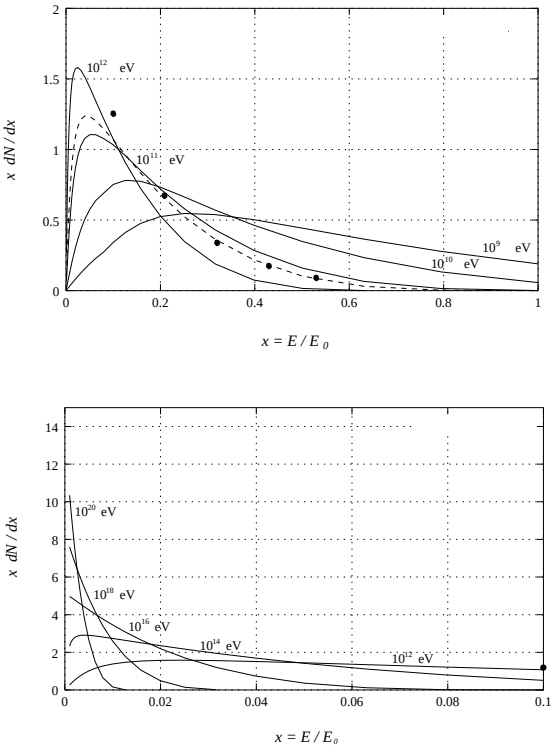

Fig. 2. x-distribution of Model-2, $x(dN/dx)$, for various primary energies E_0. The chain line in the upper figure is the scaling function of eq.(2) in the text. Full circles are experimental data of $p + p \rightarrow \pi^{ch} + X$ at $s^{1/2} = 20$ GeV[17], where the scaling law is valid. Model-2 shows the strong violation of Feynman scaling law both in the forward region and in the central region at high energies. The lower figure shows that the distribution in the forward region shrinks distinctly, in particular at highest energies.

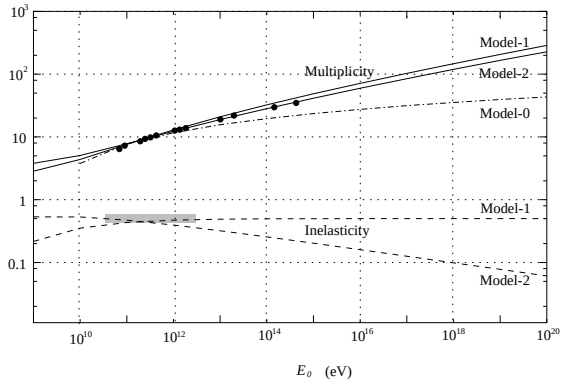

Fig. 3. Energy dependence of charged multiplicity and that of total inelasticity, predicted by the models in Table 1. Experimental data of average charged multiplicity (full circles) is from bubble chambers, ISR and S$\bar{p}p$S, compiled in Ref.[10]. The multiplicity is not different so much between Model-1 and Model-2. Model-2 describes the experimental data better than Model-1, because Model-2 has the best-fit parameters to describe the rapidity density distribution. Inelasticity is decreasing in Model-2, while it is constant (=0.5) for Model-0 and Model-1. The shadowed area indicates the region where the Feynman scaling law, *i.e.* $< K >= 0.5$, is verified by the experiments within the experimental errors.

where the factor 3/2 is due to charge independence on the assumption that all the produced particles are pions. It shows that the inelasticity decreases considerably in Model-2 at high energies while it is constant (*i.e.* 0.5) in Model-0 and in Model-1.

2.3 Models employed in simulations

It is also interesting to see how the formulated distribution is reproduced by the models which are used recently in simulations of atmospheric cosmic-ray diffusion. In Fig. 4 we compare the pseudo-rapidity density distributions, compiled by J. Knapp *et al.*,[18] which are predicted by the simulation codes of UA5 code,[19] VENUS,[20] QGSJET,[21] SIBYLL,[22] HDPM[23] and DPMJET,[24] with those of Model-0, -1 and -2. Note that the pseudo-rapidity density by simulations is for NSD (non-single-diffractive) events while that of the calculation is for all inelastic events.

The following observations can be made from Fig. 4.
(1) In the central region all the distributions are similar except that of HDPM.
(2) In the middle region QGSJET, VENUS, DPMJET predict higher density appreciably than that of Model-2.
(3) In the forward region all the model predictions are almost consistent.
(4) UA5 code predicts the most consistent distribution with that of Model-2.
(5) The difference of the rapidity densities, predicted by respective simulation models, is not negligibly small.
(6) The rapidity density of the QGSJET model, which is used frequently at present in simulations of cosmic-ray phenomena, is almost between those of Model-1 and Model-2.

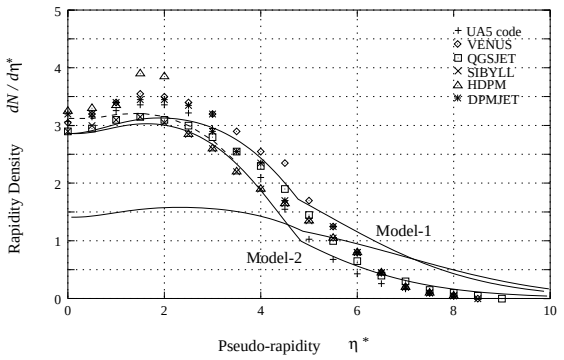

Fig. 4. Pseudo-rapidity density distributions at $s^{1/2} = 546$ GeV. Plots are by the simulation models (UA5 code, VENUS, QGSJET, SIBYLL, HDPM and DPMJET). The data by the simulations are based on the NSD (non-single-diffractive) events, while those by Model-0, Model-1 and Model-2 (solid lines) are for all inelastic events. The chain line is that of Model-2 which is corrected for NSD events.

§3. Highest energy air showers

In this section we examine whether the formulated energy distribution is compatible or not with the data of extremely high energy ($\sim 10^{20}$ eV) air showers. Since the energy dependence of nuclear interaction characteristics appears in most distinct way at these energies, the examination might be made without ambiguity.

3.1 Air showers

A high energy primary cosmic-ray proton, incident upon the top of the atmosphere, makes a nuclear collision with an atmospheric nucleus, and many particles — one surviving particle and a number of produced particles — are produced through the collision. The surviving particle, either a proton or a neutron, repeats inelastic collisions in the atmosphere. The inelastic cross section of the nucleon-air collisions increases with the incident energy.

The produced particles are assumed to be pions. The energy distribution of produced pions is given by eq.(2) of $N-N$ collisions, because the effect of the air nucleus target appears only in the backward region.The diffusion of cosmic rays in the atmosphere is governed by the high energy particles, produced in the forward region. The charged pions among the produced pions make nuclear collisions in the atmosphere again. The collision mean free path of charged pions has the same energy dependence as that of nucleons. We neglect decays of charged pions into muons.

The multiple particle production, induced by a charged pion, has essentially the same characteristics as the ones by a nucleon, which is confirmed within the errors of the experimental data in low energy region.[8)]

That is, the final state of the collision consists of one surviving pion and produced pions whose energy distribution is the same as the one of proton collisions. The differences are that the inelastic cross section of pion is smaller than that of proton, and that the surviving pion has a probability to be a neutral pion (called the 'charge exchange' process). The charge exchange process is important because the surviving particle has larger energy compared with the produced particles in most of the cases.

The neutral pions among the produced pions and those through the charge exchange process decay into γ-rays which produce a number of electromagnetic component, electrons and photons, via electromagnetic cascade process.

3.2 Assumptions for elementary processes

Following the above scenario we formulate the elementary processes.

(1) Inelastic collision mean free path

We formulate the energy dependence of the mean free paths of $N-air$ and $\pi-air$ collisions in the following way.[25–27)]

$$\lambda_N(E_0) = \lambda_N \left(\frac{E_0}{B}\right)^{-\beta}$$

$$\lambda_\pi(E_0) = \lambda_\pi \left(\frac{E_0}{B}\right)^{-\beta} \tag{3.1}$$

$$(\lambda_N = 80.0 \text{ g/cm}^2,\ \lambda_\pi = 113 \text{ g/cm}^2,\ \beta = 0.056)$$

(2) Energy distribution of produced particles

The energy distribution of *charged* produced particles in the laboratory system is given by eq.(2). That is,

$$\varphi(E_0, E)dE$$

$$= D\left(\frac{E_0}{A}\right)^{\alpha} \left[1 - \left(\frac{E_0}{A}\right)^{\alpha'} \frac{E}{E_0}\right]^{d} \frac{dE}{E} \tag{3.2}$$

$$(A = 2.0 \times 10^2 \text{ GeV},\ D = 1.67,\ d = 4.0)$$

where E_0 is the energy of the incident particle. The parameters α and α' are tabulated in Table 1.

(3) Inelasticity

According to eq.(7) the average total inelasticity is given by

$$< K >= 0.5 \left(\frac{E_0}{A}\right)^{\alpha-\alpha'}$$

That is, the average inelasticity decreases with the incident energy for Model-2.

We assume that the inelasticity K of respective events is distributed uniformly between 0 and $2 < K >$ (≤ 1.0). The distribution provides the average value of the inelasticity $< K >$.

(4) Charge exchange probability of the surviving pion is assumed to be $b = 0.3$.

3.3 Air shower size

Air shower size is defined as the total number of charged particles in the air shower at the observation level. Among the charged particles the electron component is dominant. Therefore we calculate only the electron component for the air shower size.

Table II. Cases to be discussed

Case	Scaling violation parameters α	α'	Feynman scaling law	Cross Section	Remark
A	0	0	scaling	$\beta = 0$ (constant)	$b = 0$ and $b = 0.3$
B	0	0	scaling	$\beta = 0.056$ (increasing)	
C	0.105	0.105	violated	$\beta = 0$ (constant)	Model-1
D	0.105	0.210	violated	$\beta = 0$ (constant)	Model-2

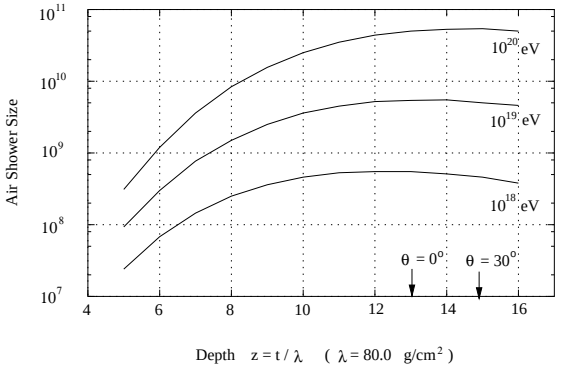

Fig. 5. Transition curve of the air shower size for the primary proton with the energy $E_0 = 10^{18}$, 10^{19} and 10^{20} eV, for Case A (Model-0 and constant cross section). The arrows indicate the depth of the sea level (1,030 g/cm^2) for the air showers with the inclination $\theta = 0°$ and 30°.

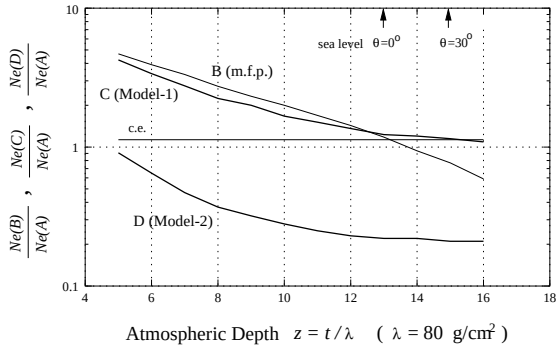

Fig. 6. Ratio of air shower size, N_e(B)/N_e(A), N_e(C)/N_e(A) and N_e(D)/N_e(A), along the depth. The cases of A, B, C and D are tabulated in Table 2. The primary energy of a proton is 10^{20} eV.

As can be seen in Appendix A, one can calculate the air shower size N_e if one can solve the diffusion equations for nucleon and pion components. It is not simple, however, to solve them taking all the processes (1) $\sim$ (4), mentioned above, into account simultaneously. Therefore we discuss the effects of respective processes one by one. That is, we calculate the cases, tabulated in Table 2, and discuss the ratio between the air shower size of each process and that of the case A.

Fig. 5 shows the transition curve of the air shower size of the case A for the primary proton with the energies $E_0 = 10^{18}$, 10^{19}, and 10^{20} eV. One can see in the figure that the air showers of 10^{20} eV are at the maximum development at sea level and that the relation $E_0/N_e \simeq 2.0$ (GeV) holds approximately, irrespective of the primary energy E_0.

The effect of the charge exchange process is examined, too, assuming the probability $b = 0.3$. The effect is almost constant over the atmospheric depth, amounting 13 %. (Fig. 6) The approximately constant effect over the depth can be explained by the facts; (1) that the probability b is included in the attenuation mean free path of pion component $\xi\mu_\pi(s)$ and in the coefficient of the pion term, and (2) that the shower development before the shower maximum is governed by $e^{\xi_0\lambda_1(s)z}$ but not by $e^{\xi\mu_\pi(s)z}$. (See Appendix A.)

Fig. 6 shows the ratio of the air shower size between the cases B, C and D and the case A, tabulated in Table 2, at the primary energy $E_0 = 10^{20}$ eV. One can see the following in the figure.
(1) Effect of the charge exchange process of the surviving pion is almost constant over the atmospheric depth, and amounts 13 %.
(2) Effect of increasing cross section is large at high altitude, but is small at sea level. (This tendency can be seen by the analytic expression of the air shower size where the increasing cross section is taken into account.)
(3) The effects of scaling violation, in Model-1 and in Model-2, have similar depth dependence, but the absolute values of them differ by five times.
(4) Model-2 gives smaller air shower size, and the attenuation of the air shower size after the shower maximum is very slow due to the small value of inelasticity.
(5) At sea level the air shower size is dependent most strongly on the energy distribution of produced particles, among the examined processes of nuclear interaction characteristics.

§4. Summary and discussions

(i) Analytical expression is given for the air shower size, by solving the diffusion equations of hadrons in the atmosphere. The equations take into account (1) the energy distribution of produced particles, formulated empirically by the data of direct observation, (2) increasing cross section of *hadron−air* collisions, and (3) the charge exchange probablity of the surviving pion. It enables us

Table III. Air shower size at sea level, expected by the formulated models, for the incident proton of $E_0 = 10^{20}$ eV

	Model-0	Model-1	Model-2	CORSIKA
size*	5.0×10^{10}	6.2×10^{10}	1.1×10^{10}	
ratio to Model-0	($\times$1.0)	($\times$1.23)	($\times$0.22)	
charge exchange	$\times$1.13	$\times$1.13	$\times$1.13	
increasing cross section	$\times$1.18	$\times$1.18	$\times$1.18	
size (expected)**	6.7×10^{10}	8.3×10^{10}	1.5×10^{10}	5.5×10^{10}

* without the processes of increasing cross section and the charge exchange.
** with the processes of increasing cross section and the charge exchange.

to discuss how the physical processes, mentioned above, affect the air shower size. These processes are the major factors to govern the diffusion of high energy cosmic rays in the atmosphere. We obtained the following observations about the size of the extremely high energy air showers.
(1) Effect of charge exchange process is almost constant ($\times$1.13) over the whole depth in the atmosphere.
(2) Effect of increasing cross section is large ($\times$ 2 $\sim$ 3) at mountain altitudes, but small ($\times$1.18) at sea level.
(3) Effect of scaling violation of Model-1 is large ($\times$ 2 $\sim$ 3) at mountain altitudes, but small ($\times$1.23) at sea level.
(4) Effect of scaling violation of Model-2 is not negligible at any depth, *i.e.* $\times$ 0.6 $\sim$ 0.4 at mountain altitudes and $\times$0.22 at sea level.

(ii) The air shower size at sea level, expected by the present calculation, is tabulated in Table 3 for the incident proton of $E_0 = 10^{20}$ eV. To calculate the expected air shower size, to which the effects of charge exchange probability and increasing cross section are included, we multiplied all the factors because the factors are close to 1.0.

(iii) M. Nagano *et al.* examined the method of energy determination of extremely high energy air showers, employed by AGASA experiment, by the simulation code of CORSIKA[23] (with QGSJET model). And they reached the conclusion that the method works well for the highest energy air showers.[28] The simulation gives $N_e = 5.5 \times 10^{10}$ for the proton-induced air showers of $E_0 = 10^{20}$ eV.We obtained $N_e = 5.5 \times 10^9$ for the proton-induced air showers of $E_0 = 10^{19}$ eV, from the figure in Ref.,[28] and multiplied it by 10. We can see the following points by comparing the value with those in Table 3.
(1) The value by the simulation is between those of Model-1 and Model-2. In this sense our calculation and the simulation are consistent each other, because we saw in Section 2 that the pseudo-rapidity density distribution by the QGSJET model is between those by Model-1 and Model-2.
(2) If we take Model-1, the energy spectrum of highest energy air showers shifts to the left (lower energy side) by a factor 1.5.
(3) If we take Model-2, which is the best-fit to the experimental data, the energy spectrum shifts to right (higher energy side) by a factor 3.7.

¿From these observations it is reasonable to conclude that the energy estimation of EHEAS has an error of factor 2 around the present value. Note that the error of energy calibration is not statistical but systematic.

Furthermore ambiguity of the energy distribution of produced particles brings the largest ambiguity to the size of extremely high energy air showers among the physical processes, discussed in this paper. Hence we have to specify the energy distribution of produced particles in multiple particle production in more detail, in order to confirm the extremely high energy cosmic rays exceeding 10^{20} eV.

(iv) The item (3) in the above paragraph makes the puzzle of extremely high energy cosmic rays more serious.The air showers with energy exceeding the GZK cut-off. Therefore it may not be irrelevant to say that Model-2 does not describe the highest energy air showers. This examination is indispensable because it is believed that the air shower size near the shower maximum is a stable parameter to be unchanged by difference of nuclear interaction characteristics.

Origin of this small size in Model-2 is due to the fact that Model-2, which is the best-fit to the present experimental data, predicts small inelasticity at high energies. For example, the value is as small as 0.2 even at $E_0 = 10^{16}$ eV. According to our previous analysis of attenuation mean free paths of hadron and (e, γ) components,[29] the inelasticity of $< K >= 0.5$ is compatible with the experimental data in the energy region of $10^{14} \sim 10^{16}$ eV.

Note added :

M. Nagano made a comment to my talk in the symposium that the energy of the air shower is estimated by the particle density at $r = 600$ m, ρ_{600}, but not by the air shower size. (Therefore the estimated energy does not depend on my argument of the air shower size.) I would like to show in this note that his comment is irrelevant, because it is not the first time for him to make this kind of comment and because an Italian physicist also made a similar comment to me in another symposium.

Let us assume two nuclear interaction models, A and B. Since we are discussing a matter of principle, we assume that the air shower sizes predicted by two models, $N_e(A)$ and $N_e(B)$, are different *appreciably*, for exam-

ple, by factor 5. According to his comment the relation $\rho_{600}(A) = \rho_{600}(B)$ must hold because ρ_{600} is related to the primary energy E_0. Needless to say, it is impossible. (I agree to the point that ρ_{600} is rather stable against a slight change of nuclear interaction characteristics, as N_e near the shower maximum is. But we cannot say that ρ_{600} reflects the primary energy E_0 directly.)

What Nagano *et al.* showed in Ref.[28] is that the method to use $\rho_{600}(A)$ works well to estimate E_0 in the framework of the model A (but not in the framework of the model B).

Of course, I agree to the point that energy estimation is made better for some experimental reasons through ρ_{600} than through N_e which is calculated from the lateral distribution of particle density.

Acknowledgment

The author thanks Prof. E.H. Shibuya of Universidade Estadual de Campinas (Brazil) and Prof. M. Tamada of Kinki University (Japan) for their helpful discussion to complete this paper.

Appendix

(Air shower size)

According to the discussion in the subsection 3.4, the air shower size is given by

$$N_e(E_0,z) = \int_0^z dz' \int_0^\infty dE\ \Pi(E,0,z-z') \times$$

$$\left[\frac{\phi(s)}{s+1}F_N(E,z') + \xi\frac{\phi(s)+2b<(1-K)^s>}{s+1}F_\pi(E,z')\right]$$

where $F_N(E,z)$ and $F_\pi(E,z)$ are the number of nucleons and pions with energy E at the depth z. And $\Pi(E_0,0,z)$ is the number of electrons ($E \geq 0$) under Approximation B.

In the case A we can solve the diffusion equations for nucleons and pions exactly, on the basis of the physical processes described in Section 2, and we have

$$N_e(E_0,z) = \frac{1}{2\pi i}\int \frac{ds}{s(s+1)}\left(\frac{E_0}{\epsilon}\right)^s L(s)\sqrt{s}K_{1,0}(s,-s)$$

$$\times\phi(s)\left[\frac{e^{\mu_N(s)z}-e^{\xi_0\lambda_1(s)z}}{\mu_N(s)-\xi_0\lambda_1(s)} + \xi\frac{\phi(s)+2b<(1-K)^s>}{\mu_N(s)-\xi\mu_\pi(s)}\right.$$

$$\left.\left\{\frac{e^{\mu_N(s)z}-e^{\xi_0\lambda_1(s)z}}{\mu_N(s)-\xi_0\lambda_1(s)} - \frac{e^{\xi\mu_\pi(s)z}-e^{\xi_0\lambda_1(s)z}}{\xi\mu_\pi(s)-\xi_0\lambda_1(s)}\right\}\right]$$

where z is measured in the unit of λ_N. (*i.e.*, $\xi = \lambda_N/\lambda_\pi$, $\xi_0 = \lambda_N/X_0$) The integration is a complex one, originated from the inverse Mellin transformation. The first line is related to the cascade functions, and the second and the third are to the π^0 production by nucleons and pions.

The terms $\mu_N(s)$, $\xi\mu_\pi(s)$ and $\xi_0\lambda_1(s)$ are related to the attenuation of nucleons, pions and electrons, respectively.

$$\mu_N(s) = -1 + <(1-K)^s>$$

$$\mu_\pi(s) = -1 + (1-b) <(1-K)^s> + \phi(s)$$

$$\lambda_1(s) = (\text{by the cascade theory})$$

where $\phi(s)$ is the Mellin transform of the energy distribution of the produced pions (eq.(2)),

$$\phi(s) = \int_0^1 x^s dx\ \varphi(E_0,E) \qquad (x = \frac{E}{E_0}),$$

and $<(1-K)^s>$ is given by

$$<(1-K)^s> = \int_0^1 (1-K)^s dK = \frac{1}{s+1}$$

1) R. Bernett et al. (Particle Data Group), Phys. Rev. **D54** (1996) 1.
2) S. Yoshida, AIP Conf. Proc. 516 (1999) 180.
3) J.W. Cronin, Nucl. Phys. B (Proc. Suppl.) 97 (2001) 3.
4) K. Greisen, Phys. Rev. Lett. **16** (1966) 748.
5) G.T. Zatsepin, V.A. Kuz'min, Sov. Phys. JETP Lett. **4** (1966) 78.
6) B. Schwartzschild, Phys. Today (Feb.) (1997) 21.
7) R. Feynman, Phys. Rev. Lett. **23** (1969) 1415.
8) T.K. Gaisser, R.J. Protheroe, K.E. Turver, T.J.L. McComb, Rev. Mod. Phys. 50 (1978) 859.
9) F.E. Taylor, D.C. Carey, J.R. Johnson, R. Kummerud, D.J. Richie, A. Roberts, J.R. Sauer, R. Shafer, D. Theriot, J.K. Walker, Phys. Rev. **D14** (1976) 1217.
10) G.L. Alner et al. (UA5 Collaboration), Z. Phys. **C33** (1986) 1; Nucl. Phys. **B291** (1987) 445; Phys. Rep. Nos.5 and 6 (1987) 247.
11) E. Pare, T. Doke, M. Haugenauer, V. Innocente, K. Kasahara, T. Kashiwagi, J. Kikuchi, S. Lazano, K. Masuda, H. Murakami, Y. Muraki, T. Nakada, A. Nakamoto, T. Yuda, Phys Lett. **B242** (1990) 531.
12) R. Haar, C. Liapis, P. Karchin, C. Biino, S. Erhan, W. Hofmann, P. Kreuzer, D. Lynn, M. Medinnis, S. Palestini, L. Pesando, M. Punturo, P. Schlein, B. Wilkens, J. Zweizig, Phys. Lett. **B401** (1997) 176.
13) F. Abe et al. (CDF Collaboration), Phys. Rev. **D41**(1990) 2330.
14) J.A. Chinellato et al., Prog. Theor. Phys. Suppl. No.76 (1983) 1.
15) A. Ohsawa, E.H. Shibuya and M. Tamada, to appear in Phys. Rev. **D**.
16) C.M.G. Lattes et al. Prog. Theor. Phys. Suppl. No.47 (1971) 1.
17) M. Adams et al., Z. Phys. **C39** (1988) 257.
18) J. Knapp, D. Heck, G. Schatz, Preprint of Forchungszentrum Karlsruhe, FZKA 5828 (1996).
19) G.J. Alner et al. (UA5 Collaboration), CERN-EP/86-213 (1986).
20) K. Werner, Phys. Rep. **232** (1993) 87.
21) N.N. Kalmykov, S.S. Ostapchenko, Yad. Fiz. **56** (1993) 105; N.N. Kalmykov, S.S. Ostapchenko, Phys. At. Nucl. **56** (3) (1993) 346; N.N. Kalmykov, S.S. Ostapchenko, A.I. Pavlov, Bull. Russ. Acad. Sci. (Physics) **58** (1994) 1966.
22) R.S. Fletcher, T.K. Gaisser, P. Lipari, T. Stanev, Phys. Rev. **D50** (1994) 5710; J. Engler, T.K. Gaisser, P. Lipari, T. Stanev, Phys. Rev. **D46** (1992) 5013.
23) J.N. Capdevielle et al., Preprint of Kernforschungszentrum Karlsruhe KfK 4998 (1992).
24) J. Ranft, Phys. Rev. **D51** (1995) 64.
25) R.A. Nam et al., Proc. 18th Int. Cosmic Ray Conf. (Banga-

lore) Vol.5 (1983)336.
26) T. Hara et al., Phys. Rev. Lett. **50** (1983) 2058.
27) M.N. Dyakonov et al., Proc. 20th Int. Cosmic Ray Conf. (Moscow) Vol.6 (1987) 147.
28) M. Nagano et al., Preprint of Forschungszentrum Karlsruhe, FZKA 6191 (1998).
29) A. Ohsawa, K. Sawayanagi, Phys. Rev. **D49** (1992) 3128-3133.